Grain refinement in a AlZnMgCuTi alloy by intensive melt shearing: a multi-step nucleation mechanism

H. T. Li[1, 2], M. Xia[1, 2], Ph.Jarry[3], G. M. Scamans[1, 2], Z. Fan[1, 2]

[1]LiME (EPSRC Centre for Innovative Manufacturing in Liquid Metal Engineering)

[2]BCAST (Brunel Centre for Advanced Solidification Technology)

Brunel University, Uxbridge, Middlesex, UB8 3PH, UK

[3]Alcan CRV, Parc Economique Centr' Alp, 725 rue Aristide Berges–BP27, 38341 Voreppe Cedex, France

ABSTRACT

Direct chill (DC) cast ingots of wrought Al alloys conventionally require the deliberate addition of a grain refiner to provide a uniform as-cast microstructure for the optimisation of both mechanical properties and processability. Grain refiner additions have been in widespread industrial use for more than half a century. Intensive melt shearing can provide grain refinement without the need for a specific grain refiner addition for both magnesium and aluminium based alloys. In this paper we present experimental evidence of the grain refinement in an experimental wrought aluminium alloy achieved by intensive melt shearing in the liquid state prior to solidification. The mechanisms for high shear induced grain refinement are correlated with the evolution of oxides in alloys. The oxides present in liquid aluminium alloys, normally as oxide films and clusters, can be effectively dispersed by intensive shearing and then provide effective sites for the heterogeneous nucleation of Al_3Ti phase. As a result, Al_3Ti particles with a narrow size distribution and hence improved efficiency as active nucleation sites of α-aluminium grains are responsible for the achieved significant grain refinement. This is termed a multi-step nucleation mechanism.

***Key Words*:** A1.grain refinement; A1. Nucleation; A1.Solidification; B1.Alloys

Bibliography information:
H.T. Li, M.Xia, Ph.Jarry, G.M.Scamans, Z.Fan, Journal of Crystal Growth 314 (2011) 285–292.

1. Introduction

In order to underline the importance of grain refinement, in direct chill (DC) casting of aluminium alloys, grain refinement can [1-3] interact with or influence the end product mechanical properties, its formability during thermo-mechanical processing, the occurrence of surface defects during downstream processing, the homogenization treatment kinetics and the anodizing properties. During casting itself, grain refinement directly influences the formation of porosity and hot tearing. The microsegregation scales as well as the macrosegregation features, especially when related to grain transport phenomena, are strongly influenced by the grain refining strategy.

Al-Ti-B master alloys as grain refiner additions are commonly added to melts for the DC ingot production of wrought aluminium alloys. However, only 1% of the added particles successfully nucleate aluminium grains and this low efficiency is undesirable not only for its immediate cost implications, but also because refiner particles may themselves be detrimental in the final microstructures [2] particularly for products intended for extrusion, deep drawing, or high performance structural applications [3]. Grain refinement theories proposed so far can be classified as either related to an enhanced heterogeneous nucleation mechanism or to a growth restriction mechanism. Nucleation based theories include phase diagram theory, peritectic hulk theory, hypernucleation theory [4, 5] and duplex nucleation theory [6, 7]. However, most of the nucleation based theories have been discredited and their greatest weakness is that they do not apply to both foundry and wrought alloys [8]. Growth restriction is generally related to the high constitutional undercooling of solute elements and is usually characterised by the growth restriction factor (GRF) [8-12]. The theoretical basis of the growth restriction theory is that restriction of the growth of already nucleated grains permits further nucleation in the undercooled melt until the total latent heat release is sufficient to cause recalescence and the loss of undercooling. Greer and co-workers developed the free growth model to understand the physical mechanism behind the low efficiency of commercial grain refiners based on the Al-Ti system [13-15]. This showed that the size distribution of grain refiner particles plays a key role on the resultant grain refinement effect.

Bibliography information:
H.T. Li, M.Xia, Ph.Jarry, G.M.Scamans, Z.Fan, Journal of Crystal Growth 314 (2011) 285–292.

Oxides are inevitably present in liquid metals and alloys in the form of oxide films and/or oxide clusters that can cause severe difficulties during casting, and become inclusions and other related defects resulting in the degradation of the mechanical properties of cast components. Extensive effort has been made to remove oxides from liquid metal prior to casting using both chemical and physical approaches [16-18]. Recently, the MCAST (Melt Conditioning by Advanced Shear Technology) [19-21] process, has been developed for conditioning liquid metal under intensive forced convection before solidification and it has been demonstrated that naturally occurring oxides can enhance heterogeneous nucleation for microstructural refinement in commercial Mg-Al alloys [20]. Oxide clusters and films are composites, where nano-scale oxide particles are embedded in a liquid metal matrix. Such oxide particles can be effectively dispersed by intensive forced convection and can be potent sites for heterogeneous nucleation since there is a good crystallographic match with the nucleated solid crystalline phases.

In this paper, we have used a specially designed experimental procedure with a lower cooling rate during solidification to demonstrate the grain refinement effect of intensive melt shearing. A standard TP-1 mould [22] and a wedge-shaped copper mould were used to assess the grain refinement induced by intensive melt shearing under varying cooling rates. A pressure filtration technique [23] combined with SEM observation and quantitative metallographic analysis was used to investigate the evolution of oxides and correlate it with the achieved grain refinement. Based on these experimental observations, a multi-step nucleation mechanism is proposed.

2. Experimental

The experimental AlZnMgCuTi alloy had the following nominal composition: Al, Zn 10.5wt %; Mg 2wt%; Cu 1.6wt%; Fe 0.35wt%; Si 0.15wt%; Ti 0.2wt%. The reason for choosing this particular composition with the titanium level at 0.2 wt.% is to ensure the formation of the Al_3Ti phase on solidification. Assessment of the liquidus temperature of the alloy could be done by adding the binary peritectic contribution of Ti to the liquidus of the hypoperitectic multicomponent alloy. However, Fortier et al. [24] mentions that for a 7046A alloy the formation temperature of Al_3Zr is 20°C higher

Bibliography information:
H.T. Li, M.Xia, Ph.Jarry, G.M.Scamans, Z.Fan, Journal of Crystal Growth 314 (2011) 285–292.

than that in the Al-Zr binary alloy. The same might be true for titanium aluminide in a binary vs a multicomponent alloy. Indeed, FactSage calculations suggest that the equilibrium temperature for Al_3Ti formation in this alloy is 729°C (Fig.1), in accordance with the trend published for Al_3Zr [24]. Depending on the nucleation conditions Al_3Ti precipitates may form at quite variable undercooling or even supercooling [25].

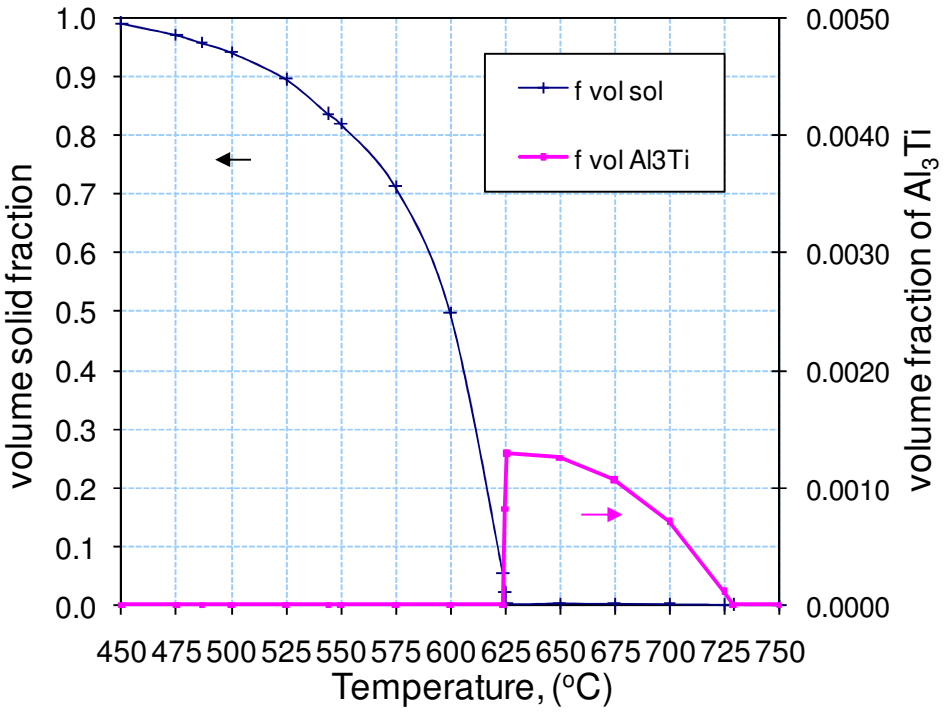

Fig. 1 *Calculated solid fraction and volume fraction of Al_3Ti in AlZnMgCuTi alloy using Factsage software.*

For all the cases with melt conditioning, the shearing temperature of the MCAST unit was set at 650°C and the temperature of the melting furnace was set at 750°C. Melt conditioning was carried out for 60 seconds at a shearing speed of 500rpm.

To eliminate the influence of pouring operation on the resulting solidification microstructure, a specially designed experimental procedure is shown in the experimental flow chart in Fig.2. A mild steel mould, of which the dimensions and the corresponding cross section for grain size assessment

Bibliography information:
H.T. Li, M.Xia, Ph.Jarry, G.M.Scamans, Z.Fan, Journal of Crystal Growth 314 (2011) 285–292.

are schematically shown in Fig.3a, wrapped with insulation and coated with boron nitride was preheated to 650°C. For the case with melt conditioning, the melt was poured into the MCAST unit at 750°C and transferred into a preheated mild steel mould after shearing for 60 seconds. For the alloy without melt conditioning, the melt was cooled to 650°C (from 750 °C) and isothermally held at 650°C for 30 minutes, and was then transferred into a preheated mild steel mould. After the melts were transferred into two mild steel moulds, respectively, the two mild steel moulds were isothermally held at 650°C for additional 3 minutes in a well preheated electrical resistance furnace. During isothermal holding, the temperature of the melts was monitored by a *K* type thermocouple to make sure the temperature of the melt was within 650±2°C. The thermocouple used was calibrated against the melting temperature for pure Al (99.9wt.%). The two mild steel moulds were then taken out from the holding furnace and air cooled to room temperature.

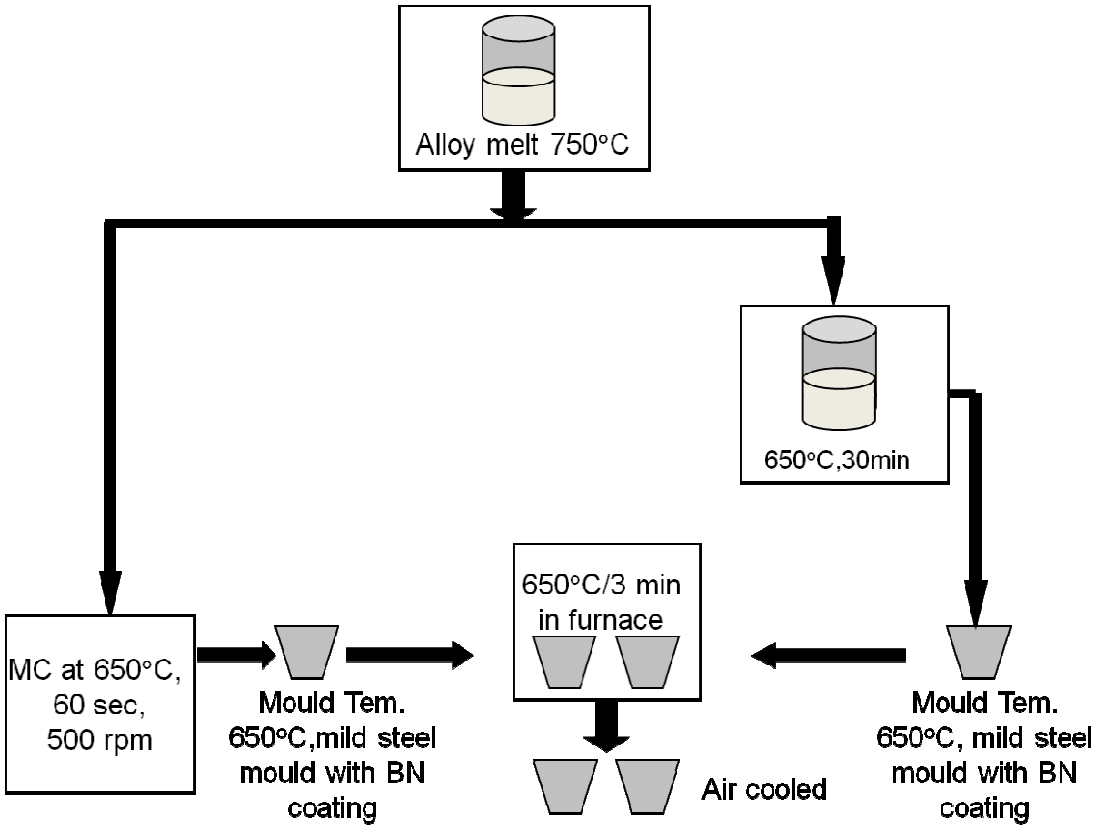

Fig. 2 *Flow chart of specially designed solidification experiment using mild steel mould.*

Bibliography information:
H.T. Li, M.Xia, Ph.Jarry, G.M.Scamans, Z.Fan, Journal of Crystal Growth 314 (2011) 285–292.

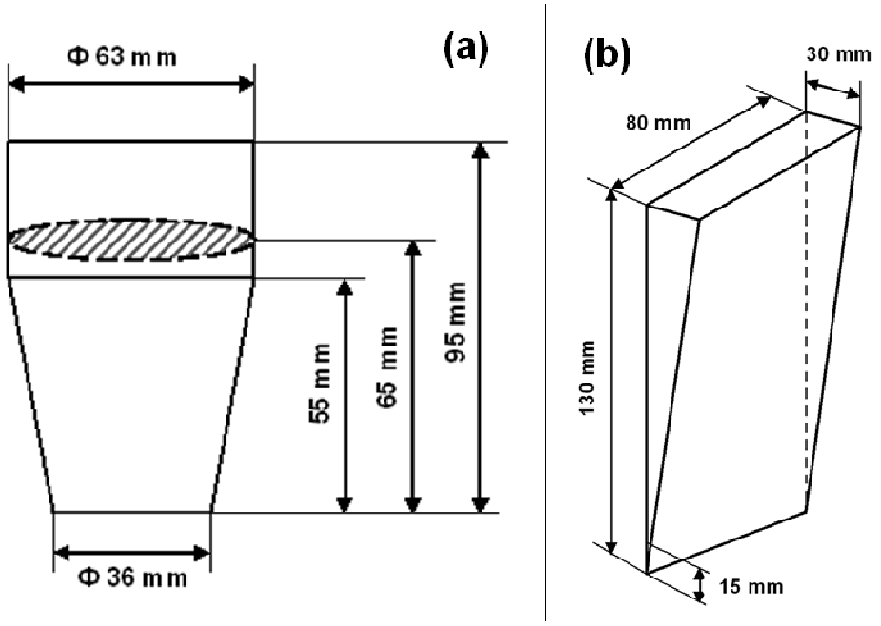

Fig. 3 *Schematic representation of the dimensions of (a) mild steel mould and (b) wedge-shaped copper mould samples and the cross section locations, where grain size was evaluated.*

A standard TP-1 mould [22] and a wedge-shaped copper mould were used to evaluate the grain refinement effect of melt conditioning under intermediate and high cooling rates, respectively. The geometry of the wedge-shaped copper mould sample is shown in Fig. 3b. Three different processing schemes were used for TP-1 samples with the same casting temperature all at 650°C, as presented in Fig. 4. For the sample without melt conditioning, the melt was air cooled to 650°C from 750°C and then cast into a TP-1 mould (scheme A in Fig. 4); for the samples with melt conditioning, two different melt conditioning processes were adopted. One was sheared at 650°C isothermally for 60s after the melt temperature had been air cooled to 650°C and then poured into MCAST unit (scheme B in Fig. 4). The other one was sheared immediately after the melt was poured into MCAST unit from 750°C, including two consecutive stages for 60s in total: continuous cooling and shearing from 750 to 650°C and subsequent isothermal shearing at 650°C (scheme C in Fig. 4). In Fig. 4, the calculated volume fraction of Al_3Ti against temperature by Factsage software is also included (same as Fig. 1) to facilitate the understanding of the development of Al_3Ti during different processes. For the wedge-

Bibliography information:
H.T. Li, M.Xia, Ph.Jarry, G.M.Scamans, Z.Fan, Journal of Crystal Growth 314 (2011) 285–292.

shaped copper mould samples, scheme A and C were used for the cases with and without melt conditioning, respectively.

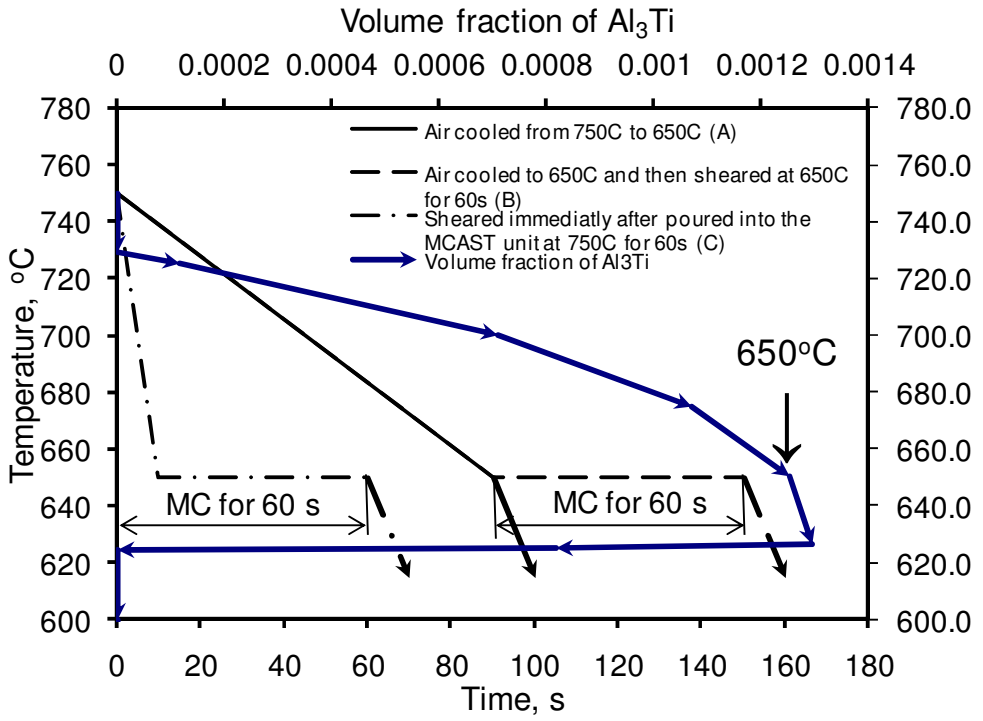

Fig. 4 *Processing schemes used for TP-1 and wedge-shaped samples overlaying with the calculated volume fraction of Al_3Ti against temperature by Factsage software. For the sample without melt conditioning, the melt was air cooled to 650°C from 750°C and then cast into a TP-1 mould (scheme A). For the melt conditioned samples, two different processes were adopted. One was sheared at 650°C isothermally for 60s after the melt temperature had been air cooled to 650°C and then poured into MCAST unit (scheme B). The other one was sheared immediately after the melt was poured into MCAST unit from 750°C, including two consecutive stages for 60s in total: continuous cooling and shearing from 750 to 650°C and subsequent isothermal shearing at 650°C (scheme C).*

The metallographic samples for optical microscopy and scanning electron microscopy (SEM) were prepared using standard metallographic procedures. The samples were sectioned as shown in Figs. 3a and 3b. The TP-1 sample was sectioned perpendicular to its axis 38mm from its base. The samples for

grain size measurement were anodized with Barker's reagent (4% HBF4 in distilled water) and then viewed under polarized light using a Zeiss optical microscope with an Axio Vision 4.3 image analysis system. The mean linear intercept technique was used to measure the grain size.

A model alloy Al-20Zn-0.05Ti was subjected to pressure filtration to analyse oxides in the melt with/without melt conditioning. The reason for choosing this alloy chemistry is to decrease the liquidus of the Al-Zn alloy to the same as the experimental wrought alloy and with a similar oxide formation and a simplified composition. The filtration crucible was preheated to ~ 300-350°C, to reduce heat loss during transfer of the liquid alloy. Filtered samples containing the concentrated oxides within the metal (~ 5 mm in thickness) in contact with the filter were sectioned, mounted, and polished for metallographic examination. Scanning electron microscopy (SEM) was carried out with a field emission gun Zeiss Supera 35 machine, equipped with an energy dispersive spectroscopy (EDS) facility and operated at an accelerating voltage of 5-20 kV.

3. Results

3.1 Specially designed experiment demonstrating grain refinement effect by intensive melt shearing

Fig. 5 shows the microstructures of sheared and non-sheared mild steel mould samples showing that the grain size was refined after intensive melt shearing. The grain size was decreased to about 260 μm after intensive melt shearing compared to 620μm for non-sheared sample. The chilled grains adjacent to the mould wall and coarse equiaxed grain structure were observed in the non-sheared sample (Figs. 5a and 5b). For the sheared sample, chilled grains adjacent to the mould wall were not observed and the grain structures both near the edge and in the interior were finer and more uniform as shown in Figs. 5c and 5d.

Fig. 5 shows the microstructures of sheared and non-sheared mild steel mould samples showing that the grain size was refined after intensive melt shearing. The grain size was decreased to about 260 μm after intensive melt shearing compared to 620μm for non-sheared sample. The chilled grains adjacent to the mould wall and coarse equiaxed grain structure were observed in the non-sheared sample (Figs.

5a and 5b). For the sheared sample, chilled grains adjacent to the mould wall were not observed and the grain structures both near the edge and in the interior were finer and more uniform as shown in Figs. 5c and 5d.

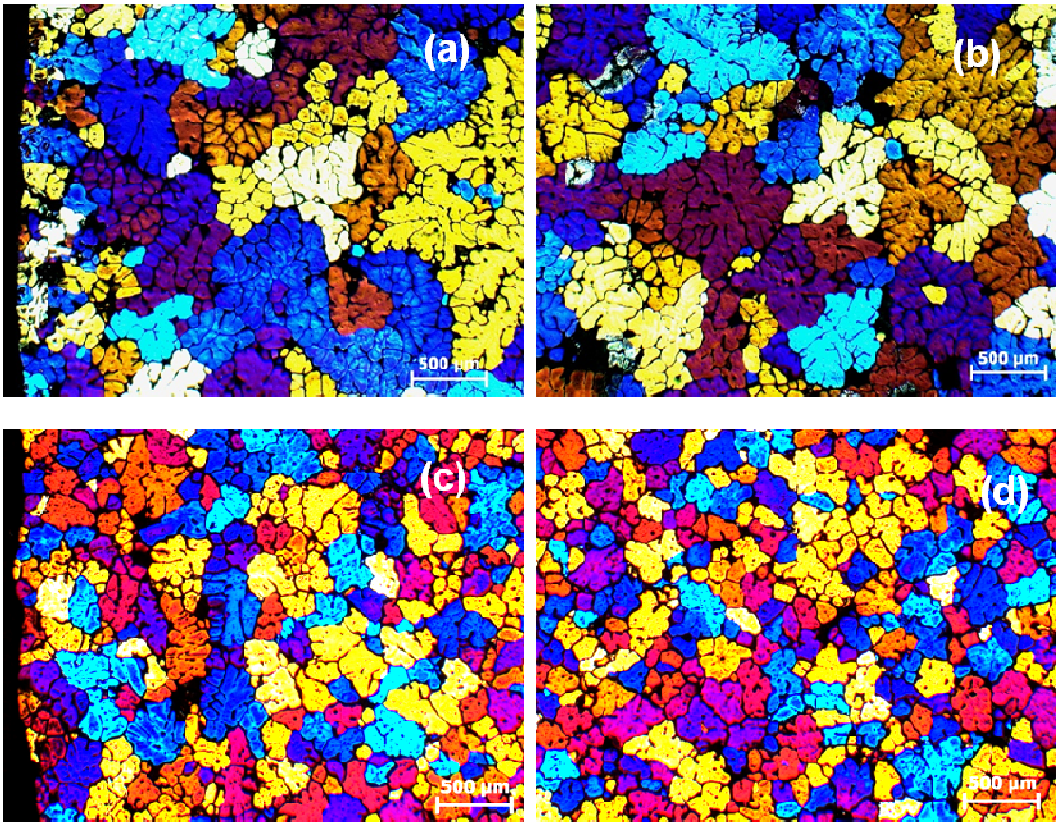

Fig. 5 *Polarised light micrographs of (a) edge area and (b) middle of non-sheared mild steel mould sample; (c) edge zone and (d) middle of sheared mild steel mould sample.*

3.2 Grain size as a function of cooling rate with and without shearing

Fig. 6 shows typical optical micrographs viewed under polarized light of the TP-1 samples cast at 650 ^{o}C, with and without melt shearing. For the sample without melt conditioning (processing scheme A in Fig.4), the average grain size was 123±24µm, (Fig. 6a); for the sample in Fig. 6b, after the melt temperature was air cooled to 650^{o}C, then poured into MCAST unit and melt conditioned (scheme B in Fig.4), the grain size was 120±21 µm almost the same as in Fig. 6a; however, in the case of the

Bibliography information:
H.T. Li, M.Xia, Ph.Jarry, G.M.Scamans, Z.Fan, Journal of Crystal Growth 314 (2011) 285–292.

sample melt conditioned with melt directly transferred into the MCAST unit from 750 ^{o}C (scheme C in Fig.4), the grain size was reduced to 48±3.5 µm (Fig. 6c.).

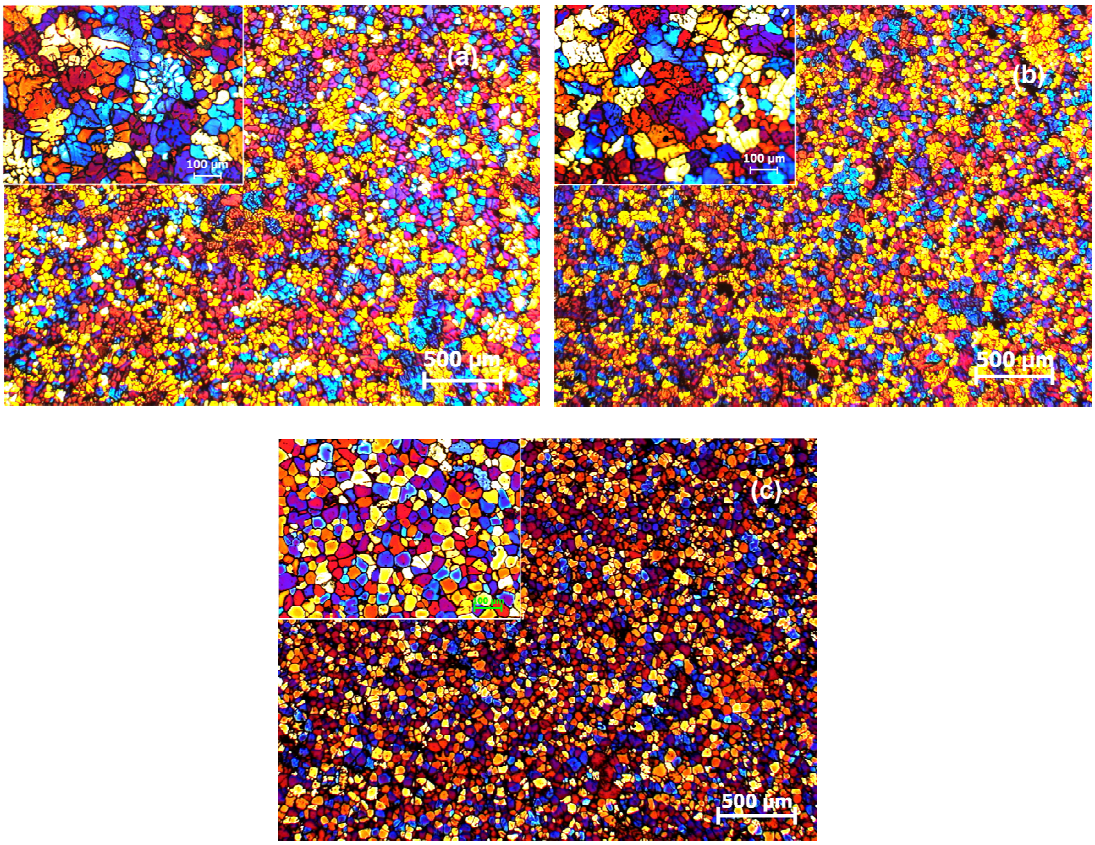

Fig. 6 *Grain structures in TP-1 samples: (a) air cooled to 650 ^{o}C from 750^{o}C and cast without shearing (scheme A in Fig.4), grain size: 123±24µm; (b) air cooled to 650^{o}C and then sheared (scheme B in Fig.4), grain size: 120±21µm; (c) Poured into MCAST unit at 750^{o}C and then sheared (scheme C in Fig.4), grain size: 48±3.5µm*

Bibliography information:
H.T. Li, M.Xia, Ph.Jarry, G.M.Scamans, Z.Fan, Journal of Crystal Growth 314 (2011) 285–292.

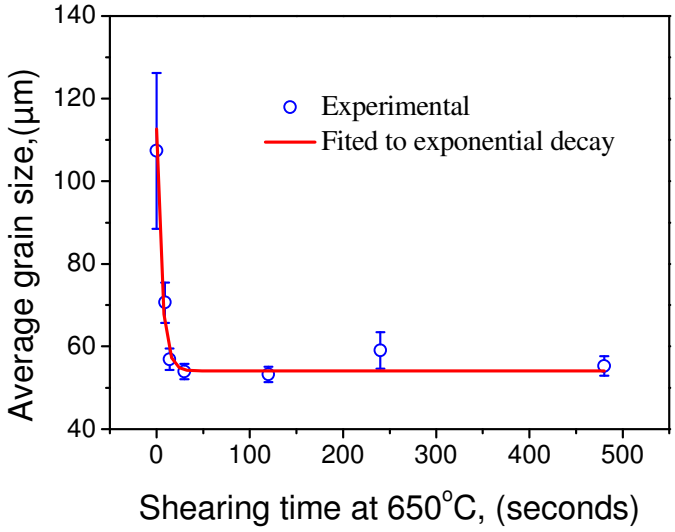

Fig. 7 *Grain size as a function of shearing time in TP-1 samples with the alloy melts directly transferred into the MCAST unit (scheme C in Fig. 4)*

Fig. 7 shows the effect of shearing time on grain size of TP-1 samples with the alloy melts directly transferred into the MCAST unit (scheme C in Fig. 4). The plot of grain size against shearing time fits an exponential decay function, showing that the grain size reaches a plateau after a period of rapid decrease beyond a critical value, that is about 10~20seconds in the current study.

The grain refinement effect of intensive shearing in the tip part of wedge-shaped samples, where a very high cooling rate of 1000°C/sec [26] was achieved, can be seen in Fig. 8. There was an almost total absence of columnar dendritic grains at the edge of the melt conditioned sample (Fig. 8b) in contrast to the readily observed columnar grains at the edge zone of the sample without melt conditioning (Fig. 8a).

Bibliography information:
H.T. Li, M.Xia, Ph.Jarry, G.M.Scamans, Z.Fan, Journal of Crystal Growth 314 (2011) 285–292.

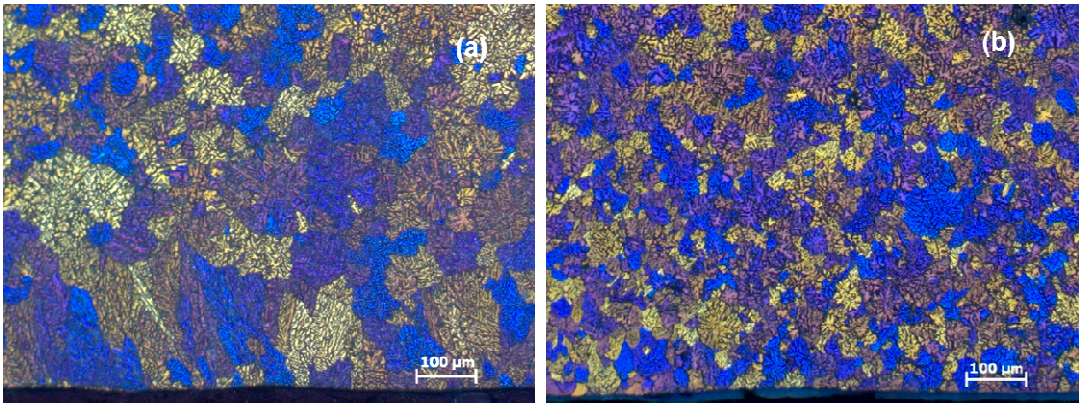

Fig. 8 *Grain structures in the tip part of wedge-shaped samples of experimental alloy: a. without shearing (scheme A in fig. 4), showing columnar dendrites in the location close to the edge of sample; b. with shearing (scheme C in Fig. 4), showing equiaxed grains throughout the cross section of sample.*

Fig. 9 compares the sensitivity of grain size to the variation of cooling rate with and without melt conditioning. It can be seen clearly that the grain refinement effect by intensive melt shearing occurs across the cooling rate range examined and is more pronounced under the conditions of lower cooling rate during the solidification process.

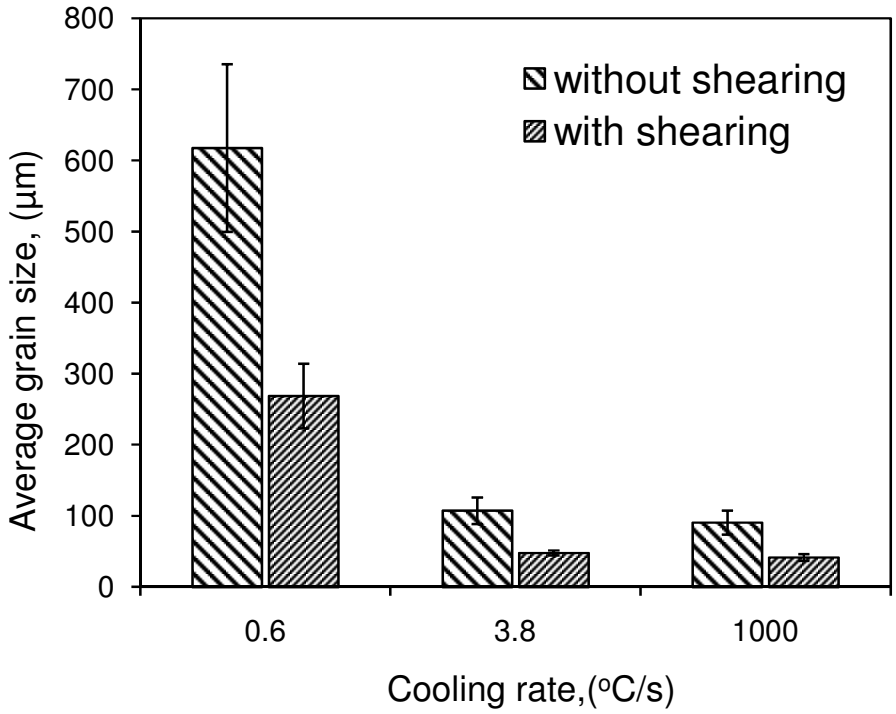

Bibliography information:
H.T. Li, M.Xia, Ph.Jarry, G.M.Scamans, Z.Fan, Journal of Crystal Growth 314 (2011) 285–292.

Fig. 9 *Grain size as a function of cooling rate, with and without shearing.*

3.3 Characterisation of Al_3Ti intermetallics and oxide particles

Detailed SEM observations were carried out using TP-1 samples with and without melt conditioning (scheme C and scheme A in Fig. 4). Fig. 10a shows that Al_3Ti intermetallic particles can be readily observed within the interior of refined grains. Comprehensive SEM observations indicated that there is an association between the intermetallic Al_3Ti particles and oxide particles, as shown in Fig. 10b, where a typical Al_3Ti intermetallic particle is associated with an oxide particle located in the centre of an α-aluminium grain. The size distribution of Al_3Ti intermetallic particles in TP-1 samples with (scheme C in Fig. 4) and without (scheme A in Fig. 4) melt conditioning is plotted in Fig. 11, showing that the Al_3Ti particles with melt conditioning have a narrower size distribution compared to the sample without melt conditioning. For instance, the size frequency of the Al_3Ti particles frequently observed within α-aluminium grains in the sheared TP-1 sample was 78.3% in the range of 6~20μm, compared to the value for the sample without shearing of only 42.7%.

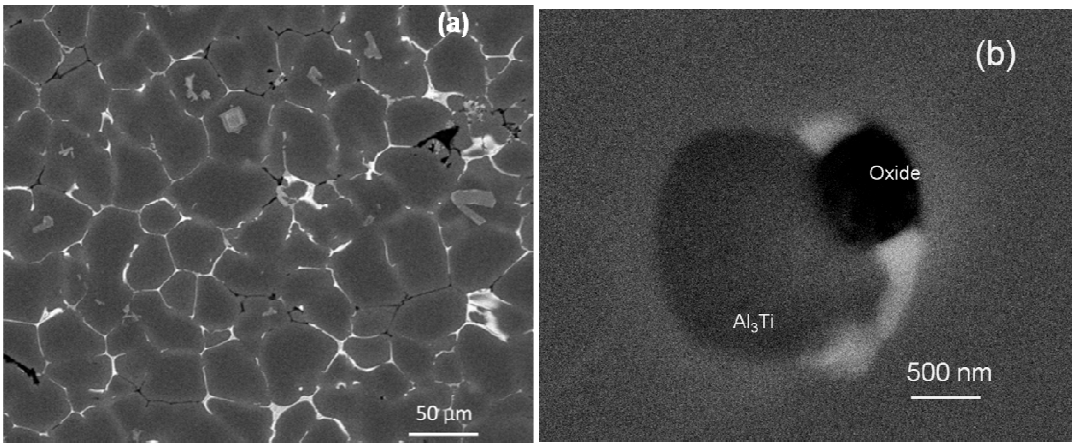

Fig. 10 *(a) SEM backscattered electron image of grain structure showing frequently observed Al_3Ti intermetallics inside the grain interior in sheared TP-1 sample, with melt directly poured into MCAST unit at 750°C; (b) A typical high magnification SEM image indicating an association between Al_3Ti and oxide particles.*

Bibliography information:
H.T. Li, M.Xia, Ph.Jarry, G.M.Scamans, Z.Fan, Journal of Crystal Growth 314 (2011) 285–292.

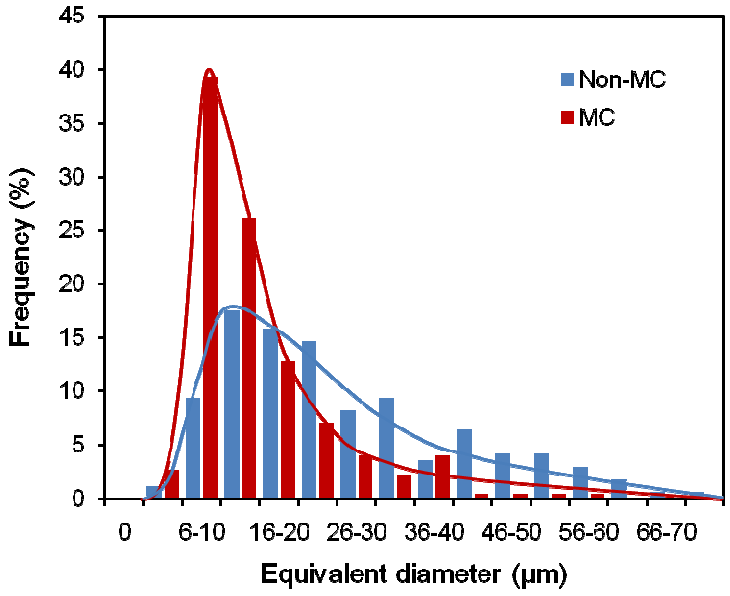

Fig. 11 *Size (equivalent diameter) distribution of Al_3Ti intermetallic particles formed in TP-1 samples with and without shearing.*

Figs. 12 and 13 show oxides in the alloy melt of Al-20Zn-0.05Ti, with and without melt conditioning. Without melt conditioning, oxides in alloy melt are in the form of oxide films or oxide clusters, as shown in Figs. 12a-c. Within films or clusters, crystalline oxide particles with sub-micron size are held together by capillary force [20] and each individual particle is surrounded by other particles rather than the aluminium matrix (Fig. 12c). The SEM-EDXS spectrum shown in Fig. 12d suggests that the oxides formed in the model alloy could be Zn-spinel. After melt conditioning, it can be seen from Fig. 13 that oxides are in the form of dispersed individual particles, which are embedded in the aluminium alloy matrix.

Bibliography information:
H.T. Li, M.Xia, Ph.Jarry, G.M.Scamans, Z.Fan, Journal of Crystal Growth 314 (2011) 285–292.

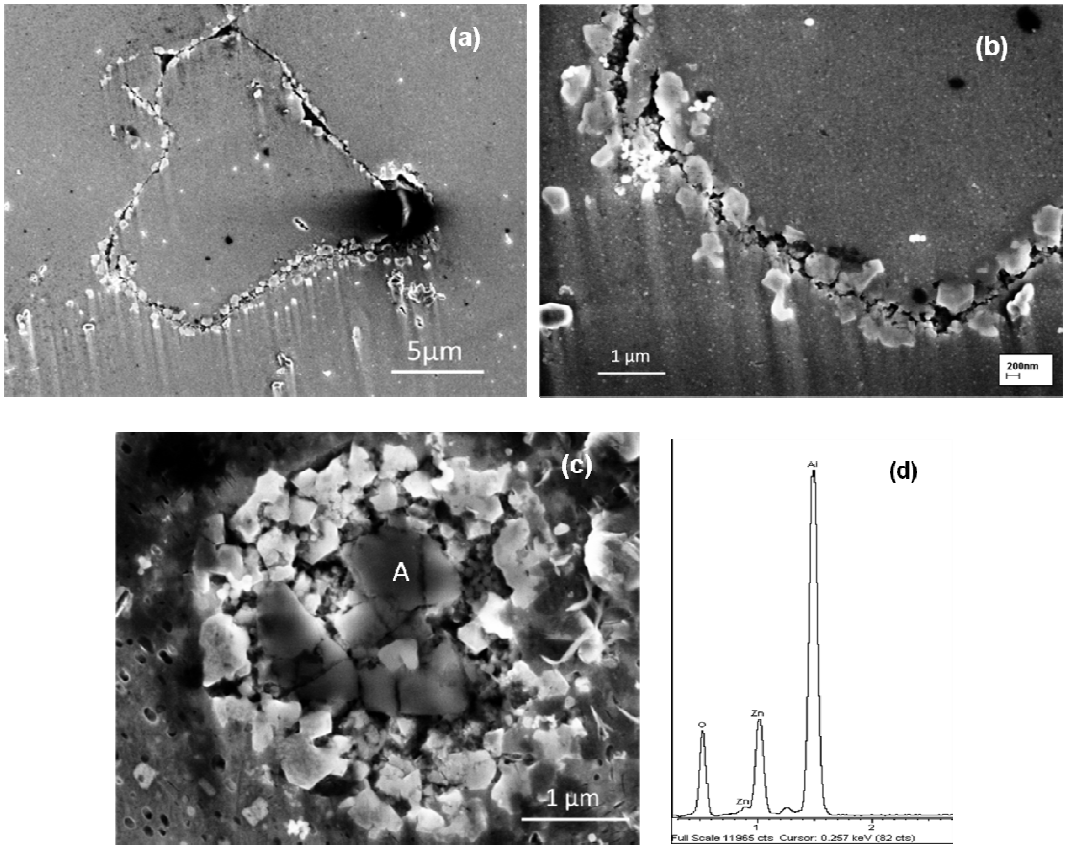

Fig. 12 *SEM images showing typical morphology of oxides in non-sheared and filtered sample of Al-20Zn-0.05Ti with: (a) low and (b) high magnification images of oxide film and (c) oxide clusters, both of which consist of individual oxide particles with sub-micron size; (d) a typical EDS spectrum of individual oxide particles marked by "A" in (c), suggesting it possibly being Zn-spinel phase.*

Bibliography information:
H.T. Li, M.Xia, Ph.Jarry, G.M.Scamans, Z.Fan, Journal of Crystal Growth 314 (2011) 285–292.

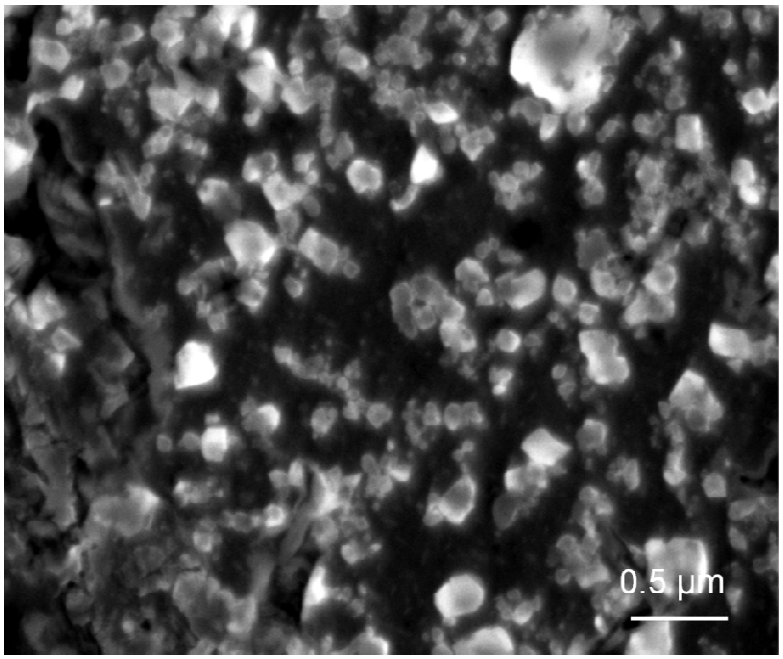

Fig. 13 *A typical SEM image of oxides in sheared and pressure filtered sample of Al-20Zn-0.05Ti showing individual dispersed oxide particle uniformly distributed in Al matrix.*

4. Discussion

For non-sheared samples, the grain size was coarser and chill zones of finer grain size were found compared to the sheared samples where the grain size was finer and uniform across the entire sample. This difference in grain structure can be understood as without melt conditioning, nucleation behaviour was triggered by thermal undercooling through the mould wall, whilst after melt conditioning, nucleation occurred throughout the whole volume of the sample by enhanced heterogeneous nucleation and resulted in homogeneous solidification.

Fluid flow during melt conditioning has been analysed previously [27-29]. The MCAST unit has a pair of screws co-rotating inside a barrel. The screw profiles are fully intermeshing and self-wiping and fluid flow is characterized by a high shear rate and a high intensity of turbulence, with a cyclic variation of shear rate. During the melt conditioning, there is an enormous amount of changing interfacial area, providing enhanced heat transfer and strong dispersive mixing. Thus, the melt with

Bibliography information:
H.T. Li, M.Xia, Ph.Jarry, G.M.Scamans, Z.Fan, Journal of Crystal Growth 314 (2011) 285–292.

intensive shearing is extremely uniform in terms of composition fields, thermal conditions and dispersed individual oxide particles.

For an oxide particle to act as a nucleus for Al_3Ti there should be good crystallographic matching. Al_3Ti has a tetragonal structure based on an ordered cubic close packed (ccp) structure [14]. Each of the oxides possibly formed in the experimental alloy melt, γ-Al_2O_3, MgO, $ZnAl_2O_4$ and $MgAl_2O_4$, has a similar cubic structure [30-33]. Based on reported lattice parameters and the expression of interatomic spacing misfit $f=[(d_2-d_1)/d_2]\times100$, where d_2 and d_1 are interatomic spacing of Al_3Ti and each individual oxide phase, respectively, the estimated interatomic misfit f along the closely packed directions between Zn-spinel/Mg-spinel and Al_3Ti are only 0.84% /0.92%, respectively. This means that both Zn-spinel and Mg-spinel could be good substrates for the nucleation of the Al_3Ti phase. In a much more recent investigation on the formation of oxides in Al-6Zn-XMg (X=0 and 2 wt.%) alloys, Zn-spinel and Mg-spinel were detected on the Al-6Zn and Al-6Zn-2Mg alloy samples, respectively [34]. In our experimental wrought alloy, the oxide formed is more likely to be Mg-spinel due to the relatively high magnesium content. With melt conditioning, dispersed Mg-spinel particles in the alloy melt may act as active nucleation sites for Al_3Ti particles. When the alloy melt was poured into the MCAST unit from 750^{o}C (scheme C in Fig. 4) in the current study, the existing oxides in the alloy melt were dispersed within a few seconds. Based on the thermodynamic calculation using Factsage software, the formation equilibrium temperature of Al_3Ti intermetallic phase in the experimental alloy, can be estimated as 729 ^{o}C (Fig. 1). Hence Al_3Ti would be anticipated to precipitate below this temperature. Due to the good crystallographic match between oxide and Al_3Ti phases as discussed above, Al_3Ti particles would preferably nucleate on oxide particles at relatively low undercooling. This applies for all the melt conditioned samples in the present study except for the case, where the melt temperature was air cooled to 650 ^{o}C and then poured into the MCAST unit (Fig. 6b, scheme B in Fig. 4). Because of the homogeneous thermal and compositional fields resulting from melt conditioning, Al_3Ti particles tend to be equiaxed and with a narrower size distribution, as evidenced by the quantitative metallographic analysis results shown in Fig. 11. Without melt conditioning, the

Bibliography information:
H.T. Li, M.Xia, Ph.Jarry, G.M.Scamans, Z.Fan, Journal of Crystal Growth 314 (2011) 285–292.

nucleation of Al_3Ti was mainly triggered by thermal undercooling and as a result, Al_3Ti particles exhibited a faceted morphology and with a wider size distribution, as indicated in Fig. 11.

The respective roles of temperature gradient and nuclei density on the columnar to equiaxed transition (CET) have been well established since Hunt's pioneering work published in 1984 [35]. The role of a grain refining additive is, in essence, to promote the CET [3]. In the modelling work on grain refinement by addition of inoculants [13, 15], the isothermal melt model was adopted in which macroscopic temperature gradients were absent, which is a reasonable assumption for air-cooled steel moulds adopted in the specially designed procedure (Fig. 2). At higher gradients such as in the case of wedge-shaped samples a higher nuclei density is necessary in order to obtain the CET (Fig. 8).

With melt conditioning, dispersed oxide particles and thereby enhanced nucleation of Al_3Ti intermetallic particles with a narrower size distribution will enhance the heterogeneous nucleation of α-aluminium phase. Greer and co-workers developed the free growth model, based on the Al-Ti-B grain refiner system in which TiB_2 particles have high potency of inoculant for α-aluminium [13, 15]. It was concluded that the grain refinement achieved is determined by a free-growth condition in which growth undercooling, ΔT_{fg}, is inversely proportional to the particle diameter of inoculants, d

$$\Delta T_{fg} = {}^{4\sigma}/_{\Delta S_v}\, d \qquad (1)$$

where σ is the solid-liquid interfacial energy and ΔS_v is the entropy of fusion per unit volume. More importantly, in their modelling, based on the understanding of recalescence limiting the number of active nucleation particles and therefore the number of grains, the size distribution of grain refiner particles rather than the size in single fixed value was treated as input. To achieve this, spatially dispersed grain refiner particles throughout the bulk melt are necessary and either settling or agglomeration behaviour of grain refiner particles should be avoided. In other words, the existence of potent nucleating agents may not necessarily lead to grain refinement in the solidified microstructure. For effective grain refinement of a given alloy composition, the potent nucleating particles need to have sufficient numbers, favourable particle size and size distribution. In present work, intensive melt

Bibliography information:
H.T. Li, M.Xia, Ph.Jarry, G.M.Scamans, Z.Fan, Journal of Crystal Growth 314 (2011) 285–292.

shearing can disperse the oxide films and clusters into individual oxide particles which promote the nucleation of Al_3Ti particles on these oxide particles. As a consequence, Al_3Ti particles with a compact and equiaxed morphology and a narrower size distribution were obtained, which in turn enhanced heterogeneous nucleation of α-aluminium grains throughout the entire volume of alloy melt. As a result, significant grain refinement effects can be achieved by intensive melt shearing. This grain refinement mechanism is termed a multi step nucleation mechanism.

The argument of the enhanced heterogeneous nucleation by Al_3Ti through a multi-step nucleation mechanism is also supported by the result shown in Fig. 6b, where Al_3Ti had formed before the melt was poured into MCAST unit at 650^{o}C (scheme B in Fig. 4), so that intensive melt shearing (dispersed oxide) had no influence on the formation of Al_3Ti and hence no effect on the grain refinement. In terms of the influence of melt conditioning time when the melt conditioning time exceeds a critical value, 10~20 seconds, a sufficient number of individual dispersed oxide particles has been achieved for the heterogeneous nucleation of Al_3Ti particles. Further, increasing the melt conditioning time doesn't contribute to an enhanced heterogeneous nucleation of Al_3Ti particles on oxide particles and its size distribution. Therefore the grain size cannot be refined further (Fig. 7).

5. Concluding remarks

1) Grain refinement has been successfully achieved in an experimental wrought AlZnMgCuTi alloy by intensive melt shearing. The grain refining effect is more pronounced under the conditions of lower cooling rate during solidification processing.

2) With intensive melt shearing, the oxide films are dispersed and uniformly distributed in the alloy melt. These oxide particles can then act as active heterogeneous nucleation sites for Al_3Ti intermetallic particles providing shearing occurs during the formation of the Al_3Ti phase.

3) Following the dispersion of oxide particles by intensive melt shearing, a narrower size distribution of Al_3Ti particles is produced providing many active sites for α-aluminium nucleation resulting in a

Bibliography information:
H.T. Li, M.Xia, Ph.Jarry, G.M.Scamans, Z.Fan, Journal of Crystal Growth 314 (2011) 285–292.

finer grain size. This multi-step nucleation process, oxide to Al_3Ti to α-aluminium, is shown to be significantly enhanced by intensive melt shearing during the formation of the Al_3Ti phase

Acknowledgements

The authors deeply thank Prof. J.D.Hunt of the University of Oxford for his critical discussion and advice concerning the experimental design, Drs Y. Wang, Y. Zuo, and S. Arumuganathar from BCAST for their help with some experiments. Valuable suggestions from the reviewer are highly appreciated. Financial support for this work from EPSRC is acknowledged. HTL is also grateful to EPSRC for awarding DHPA.

References

[1] R. Nadella, D.G. Eskin, Q. Du, L. Katgerman, Prog. Mater. Sci.53 (2008) 421-480.

[2] A. L. Greer, in: B. Cantor, K. O'Reilly (Eds.), Solidification and Casting, Institute of Physics Publishing, Bristol and Philadelphia, 2003, p. 199-214.

[3] D. G. McCartney, Inter. Mater. Rev. 34 (1989) 247-260.

[4] G.P. Jones, Proceedings of the International Seminar on 'Refining and alloying of liquid aluminium and ferro-alloys', Trondheim, Norway (1985), pp. 213-228.

[5] G.P. Jones, Proceedings of the Conference on 'Solidification Processing 1987' The Institute of Metals, London (1988), pp. 496–499.

[6] P. S. Mohanty, J. E. Gruzleski, Acta Metall.Mater.43 (1995) 2001-2012.

[7] B.S. Murty, S. A. Kori, M. Chakraborty, Inetr.Mater.Rev.47 (2002) 3-29.

[8] M. Easton, D. StJohn, Metall.Mater.Trans.A30 (1999) 1613-1623.

[9]I. Maxwell, A. Hellawell, Acta Metall.23 (1975) 229-237.

[10] M. Easton, D. StJohn, Acta mater. 49 (2001) 1867-1878.

[11] M. Easton, D. StJohn, Metall.Mater.Trans.A36 (2005) 1911-1920.

[12] D. H. StJohn, P. Cao, M. Qian, M. A. Easton, Adv. Eng. Mater. 9 (2007) 739-746.

[13] A. L. Greer, A. M. Bunn, A. Tronche, P. V. Evans, D. J. Bristow, Acta Mater. 48 (2000) 2823-2835.

Bibliography information:
H.T. Li, M.Xia, Ph.Jarry, G.M.Scamans, Z.Fan, Journal of Crystal Growth 314 (2011) 285–292.

[14] T. E. Quested, Mater. Sci. Tech. 20 (2004) 1357-1369.

[15] T. E. Quested, A. L. Greer, Acta Mater. 52 (2004) 3859-3868.

[16] J. R. Davis, Molten aluminium processing and casting. ASM speciality handbook. 1993, pp. 199-230.

[17] G. K. Sigworth, S. Shivkumar, D. Apelian, AFS Trans. 139 (1989) 811-824.

[18] X. Cao, J. Campbell, Metall. Mater. Trans. A 34 (2003) 1409-1420.

[19] Z. Fan, G. Liu, Acta Mater. 53 (2005) 4345-4357.

[20] Z. Fan, Y. Wang, M. Xia, S. Arumuganathar, Acta Mater. 57 (2009) 4891-4901.

[21] M. Hitchcock, Y. Wang, Z. Fan, Acta Mater. 55 (2007) 1589-1598.

[22] TP-1. Standard Test Procedure for Aluminum Alloy Grain Refiners. The Aluminium Association, Washington, DC (1987).

[23] X. Cao, Mater. Sci. Eng. A 403 (2005) 101-111.

[24]M. Fortier, N.C. Parson, X. G. Chen, in: J. Hirsch, B. Skrotzki, G. Gottstein (Eds.), Aluminium Alloys, Their Physical and Mechanical Properties, ICAA 11, Wiley-VCH GmbH & Co. KGaA, 2008, pp.348-354.

[25] D. H. StJohn, L. M. Hogan, J. Mater. Sci. 17 (1982) 2413-2418.

[26]A. F. Norman, P. B. Prangnell, R. S. McEwen, Acta Mater. 46 (1998) 5715-5732.

[27] S. Ji, Z. Fan, M. J. Bevis, Mater. Sci. Eng. A299 (2001) 210-217.

[28] S. Ji, Z. Fan, Metall.Mater.Trans.A33 (2002) 3511-3520.

[29] A. Das, S. Ji, Z. Fan, Acta Mater. 50 (2002) 4571-4585.

[30] JCPDS. Card No.00-029-0063.International centre for diffraction data.

[31] P. Villars, L. D. Calvert, Pearson's Handbook of Crystallographic Data for Intermetallic Phases, ASM International, Materials Park, OH (1991).

[32] K. P. Surendran, N. Santha, P. Mohanan, M.T. Sebastian, Eur.Phys.J.B41 (2004) 301-306.

[33] JCPDS. Card No.21-1152. International centre for diffraction data.

[34] P. C. Chen, T. S. Shih, J. S. Chen, J. Therm. Anal. Calorim. 99 (2010) 229-235.

[35] J.D.Hunt, Mater.Sci.Eng.65 (1984) 75-83.

Bibliography information:
H.T. Li, M.Xia, Ph.Jarry, G.M.Scamans, Z.Fan, Journal of Crystal Growth 314 (2011) 285–292.